Available online at www.sciencedirect.com
ScienceDirect
International Journal of Solids and Structures 43 (2006) 6436–6452
INTERNATIONAL JOURNAL OF SOLIDS and STRUCTURES
www.elsevier.com/locate/ijsolstr

Hysteretic linear and nonlinear acoustic responses from pressed interfaces

Jin-Yeon Kim [a,*], Arturo Baltazar [b], Jong Wan Hu [c], Stan I. Rokhlin [d]

[a] George W. Woodruff School of Mechanical Engineering, Georgia Institute of Technology, Atlanta, GA 30332, United States
[b] Instituto Tecnológico de Hermosillo, División de Estudios de Posgrado Av. Tecnológico S/N, C.P. 83240, Hermosillo, Sonora, México
[c] School of Civil and Environmental Engineering, Georgia Institute of Technology, Atlanta, GA 30332, United States
[d] Laboratory for Multiscale Materials Processing and Characterization, Edison Joining Technology Center, The Ohio State University, Columbus, OH 43221, United States

Received 28 July 2005; received in revised form 15 November 2005
Available online 19 January 2006

Abstract

An analysis of the linear and nonlinear acoustic responses from an interface between rough surfaces in elastoplastic contact is presented as a model of the ultrasonic wave interactions with imperfect interfaces and closed cracks. A micromechanical elastoplastic contact model predicts the linear and second order interfacial stiffness from the topographic and mechanical properties of the contacting surfaces during a loading–unloading cycle. The effects of those surface properties on the linear and nonlinear reflection/transmission of elastic longitudinal waves are shown. The second order harmonic amplitudes of reflected/transmitted waves decrease by more than an order of magnitude during the transition from the elastic contact mode to the elastoplastic contact mode. It is observed that under specific loading histories the interface between smooth surfaces generates higher elastoplastic hysteresis in the interfacial stiffness and the acoustic nonlinearity than interfaces between rough surfaces. The results show that when plastic flow in the contacting asperities is significant, the acoustic nonlinearity is insensitive to the asperity peak distribution. A comparison with existing experimental data for the acoustic nonlinearity in the transmitted waves is also given with a discussion on its contact mechanical implication.

Keywords: Elastoplastic contact; Acoustic nonlinearity; Interfacial stiffness; Imperfect interface

1. Introduction

Since the pioneering experimental observation (Buck et al., 1978) and theoretical analysis (Richardson, 1979) on the generation of anomalously high second order acoustic nonlinearity from interfaces and cracks, there have been numerous investigations due to its potential application to the ultrasonic inspection

* Corresponding author. Tel.: +1 404 385 6601.
E-mail address: jinyeon.kim@me.gatech.edu (J.-Y. Kim).

0020-7683/$ - see front matter © 2005 Elsevier Ltd. All rights reserved.
doi:10.1016/j.ijsolstr.2005.11.006

of imperfect interfaces and cracks (Solodov et al., 1993; Hirose and Achenbach, 1993; Rudenko and Vu, 1994; Fassbender and Arnold, 1996; Nazarov and Sutin, 1997; Hirsekorn, 2001; Chen et al., 2001; Donskoy et al., 2001; Solodov and Korshak, 2002; Pecorari, 2003; Gusev et al., 2003; Biwa et al., 2004). Especially when a crack is closed, it may remain undetected by the linear ultrasonic techniques (Rokhlin and Kim, 2003) even though it can be excited ultrasonically to generate measurable second and higher order harmonic signals (Buck et al., 1978).

When the characteristic length of the imperfectness is much smaller than the wavelength, the interaction of acoustic waves with an interface can be described by the interfacial stiffness in the quasistatic approximation (Baik and Thompson, 1984). This continuum interface model is used widely in different problems where the interface plays a role, e.g. Needleman (1990) and Suo et al. (1992). Although the use of the interfacial stiffness simplifies the analysis of the complicated scattering problem, the connection between microstructural characteristics and acoustic responses from the interface is lost since the statistical and mechanical properties of the interface are represented by one lumped parameter, the interfacial stiffness. Many researchers have studied the microstructural effects on the interfacial stiffness (Baik and Thompson, 1984; Rokhlin and Wang, 1991; Nagy, 1992; Rokhlin, 1992; Drinkwater et al., 1996; Dwyer-Joyce et al., 2001; Baltazar et al., 2002; Kim et al., 2004). Recently, Pecorari (2003) extended the quasistatic approximation to the nonlinear reflection and transmission problem. To obtain the second order interfacial stiffness, the model for the elastic contact of rough surfaces (Baltazar et al., 2002) is applied. Nazarov and Sutin (1997) predicted the nonlinearity of cracked solids based on the nonlinear parameters of a single crack obtained from the elastic rough surface contact model of Greenwood and Williamson (1966). In most previous analyses, the asperity contact is assumed to be elastic. However, since the real contact area is usually only a small fraction of the nominal contact area and thus only a small number of asperities bear the contact load, the plastic yielding of contacting asperities is inevitable in an interface having a moderate level of roughness and even under a light load. As shown in Kim et al. (2004), the acoustic interaction with an elastoplastically deformed interface is quite different from that with an elastic interface. Once the plastic deformation takes place in the asperities, the original surface profile is forgotten, resulting in a new surface profile (the elastoplastic hysteresis). An accurate description of the elastoplastic contact of rough surfaces and the interaction with acoustic waves are overwhelmingly complicated. Recently, Baltazar et al. (2002) and Kim et al. (2004) proposed micromechanical models to describe the elastoplastic behavior of interfaces in the loading–unloading process. The model was used to reconstruct microstructural parameters from macroscopic interfacial stiffnesses measured during the loading–unloading cycle. Using the reconstructed surface parameters, the real area of contact was predicted successfully.

In the nonlinear acoustics, Rudenko and Vu (1994) attempted to determine the roughness height distribution from the acoustic nonlinearity of the interface. As shown in this paper, such a determination is possible only for smooth interfaces under a low pressure. Chen et al. (2001) experimentally observed the nonlinear transmission of vertically polarized shear waves through the interfaces between solids. This problem was later theoretically treated by Pecorari (2003). Most recently, Biwa et al. (2004) proposed an interesting idea to predict the acoustic nonlinearity of interfaces without analyzing the complicated elastoplastic contact problem. They assumed a simple power-law relation between the contact pressure and the displacement for calculating the first and second order interfacial stiffness that were used to predict the nonlinearity in the transmitted and reflected waves. Currently an analysis that relates the macroscopic acoustic responses from an imperfect interface to the microstructural surface parameters in consideration of realistic contact process occurring at the interface is lacking.

In this paper, the acoustic interactions with a nonlinear interface are investigated using a micromechanical elastoplastic loading–unloading model for contacting rough surfaces. From the model, the first and second order interfacial stiffnesses are calculated. The dependence of the acoustic nonlinearity of the interface on microstructural properties is predicted. The hysteretic behaviors of the interface motion and in the linear and nonlinear acoustic responses from the interface during a loading–unloading cycle are shown. Elastic and elastoplastic contacts of surfaces with various parameters are examined. From the numerical results, the loading-history dependent behavior of the acoustic nonlinearity, the feasibility of determining asperity height distribution, the role of elastoplastic deformation and the validity condition for using the simple power-law are discussed.

2. Interfaces as nonlinear relaxators

Consider two solid bodies with identical material properties which are brought into contact by applied static pressure p_0. Due to the surface roughness, the contact at the interface is microscopically imperfect, forming an initial opening displacement (or gap) δ_0 ($=Z_+ - Z_-$) between the nominal planes of the upper (Z_+) and lower (Z_-) rough surfaces as shown in Fig. 1. These lengths (δ_0, $|Z_+|$, $|Z_-|$) are assumed to be much smaller than the wavelength of the incident longitudinal wave so that the incoherent scattering due to the randomness of the interface is insignificant.

A plane longitudinal elastic wave of arbitrary shape is incident normally to the interface at which reflected and transmitted waves are produced as shown in Fig. 1. One-dimensional wave equation for the longitudinal wave motion in Z direction is

$$\frac{\partial^2 u}{\partial t^2} = c^2 \frac{\partial^2 u}{\partial Z^2}, \tag{1}$$

where u is the particle displacement, c ($= \sqrt{E/\rho}$) is the wave speed, and E and ρ are the elastic modulus and mass density respectively. The longitudinal stress (τ) is related to the displacement by

$$\tau = E\frac{\partial u}{\partial Z} - p_0. \tag{2}$$

The boundary condition at the interface (the continuity of stress) is

$$\tau(+0,t) = \tau(-0,t) = -(p_0 + \tilde{p}(t)), \tag{3}$$

where $\tilde{p}(t)$ is the dynamic pressure at the interface induced by elastic waves, which produces the dynamic opening displacement $\tilde{\delta}(t)$ given by

$$\tilde{\delta}(t) = [u(+0,t) - u(-0,t)]. \tag{4}$$

Like the total pressure, the total opening displacement is the sum of the static and dynamic contributions, $\delta_0 + \tilde{\delta}(t)$. As explained in the following section, the dynamic pressure due to the elastic wave does not always correspond to the pressure oscillating along the contact pressure-displacement curve but it is in general the local unloading pressure (Kim et al., 2004). The displacement fields in the lower and upper half spaces are written as

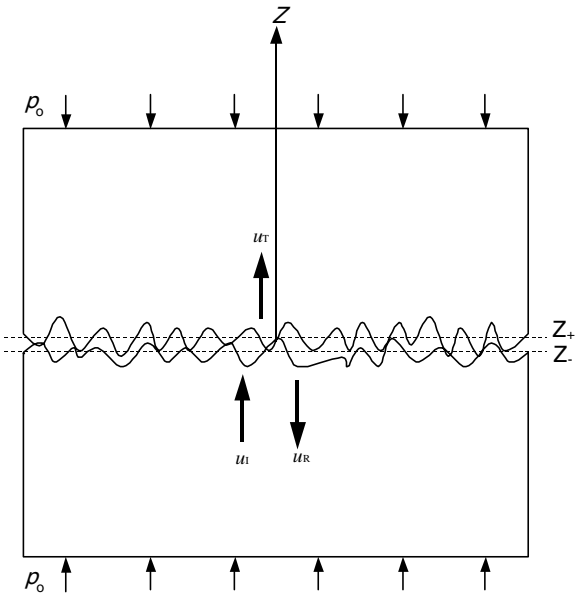

Fig. 1. A schematic showing two bodies brought into contact by applied pressure p_0 and elastic waves incident to, reflected from and transmitted through an interface formed by the contacting rough surfaces. The average planes of upper and lower rough surfaces are denoted by Z_+ and Z_-.

$$u(Z,t)=\begin{cases} u_{\mathrm{I}}(Z-ct)+u_{\mathrm{R}}(Z+ct), & Z<0,\\ u_{\mathrm{T}}(Z-ct), & Z>0, \end{cases} \tag{5}$$

where $u_{\mathrm{I}}(Z-ct)$, $u_{\mathrm{R}}(Z+ct)$ and $u_{\mathrm{T}}(Z-ct)$ are the incident, reflected and transmitted waves that satisfy Eq. (1). Eq. (3) may be rewritten as

$$\frac{1}{2}[\tau(+0,t)+\tau(-0,t)]=-\{p_0+\tilde{p}[\tilde{\delta}(t)]\}. \tag{6}$$

From Eqs. (2), (5) and (6) and the relationship $\partial u(Z\pm ct)/\partial Z=\pm c^{-1}\partial u(Z\pm ct)/\partial t$, the equation of motion of the interface in terms of its opening displacement can be obtained, i.e.

$$\frac{\mathrm{d}\tilde{\delta}(t)}{\mathrm{d}t}-\frac{2}{\rho c}\tilde{p}[\tilde{\delta}(t)]=-2\frac{\mathrm{d}u_{\mathrm{I}}(0,t)}{\mathrm{d}t}. \tag{7}$$

This is the general equation that describes the forced-vibration of a relaxator-type interface (an interface with no inertial component) (Gusev et al., 2003). For example, the nonlinear motion of a clapping interface can be described with an appropriate piecewise continuous dynamic pressure. The dynamic pressure is expanded near δ_0 for small amplitude of $\tilde{\delta}$, retaining up to the second order term

$$\tilde{p}[\tilde{\delta}(t)]\approx\left.\frac{\partial\tilde{p}}{\partial\delta}\right|_{\delta=\delta_0}\tilde{\delta}(t)+\frac{1}{2}\left.\frac{\partial^2\tilde{p}}{\partial\delta^2}\right|_{\delta=\delta_0}\tilde{\delta}^2(t)=-\overline{K}_1\tilde{\delta}(t)+\overline{K}_2\tilde{\delta}^2(t). \tag{8}$$

The negative sign in front of the first order (linear) interfacial stiffness is due to its conventional definition $\sigma=\overline{K}\Delta u$. Inserting Eq. (8) into Eq. (7) and considering a time-harmonic incidence $u_{\mathrm{I}}=U\cos[k_Z(Z-ct)]$, results in

$$\frac{\mathrm{d}\tilde{\delta}(t)}{\mathrm{d}t}+\frac{2\overline{K}_1}{\rho c}\tilde{\delta}(t)-\frac{2\overline{K}_2}{\rho c}\tilde{\delta}^2(t)=2U\omega\sin\omega t, \tag{9}$$

where k_Z $(=\omega/c)$ is the wave number of the longitudinal wave. The condition $2\overline{K}_1/\rho c>0$ ensures the stability of Eq. (9) for a weak nonlinearity. By imposing the initial condition $\tilde{\delta}(0)=0$, the transient motion is suppressed. From the solution of Eq. (9) obtained by the perturbation method (Pecorari, 2003; Biwa et al., 2004) and Eqs. (4) and (5), the reflected and transmitted waves are expressed:

$$\begin{aligned} u_{\mathrm{R}}(Z,t)=&\frac{\eta_2U^2}{\eta_1(1+4\eta_1^2)}+\frac{U}{(1+4\eta_1^2)^{\frac{1}{2}}}\cos[k_Z(Z-ct)+\theta_1]\\ &-\frac{\eta_2U^2}{(1+4\eta_1^2)(1+\eta_1^2)^{\frac{1}{2}}}\cos[2k_Z(Z-ct)+2\theta_1+\theta_2], \end{aligned} \tag{10}$$

$$\begin{aligned} u_{\mathrm{T}}(Z,t)=&-\frac{\eta_2U^2}{\eta_1(1+4\eta_1^2)}+\frac{2\eta_1U}{(1+4\eta_1^2)^{\frac{1}{2}}}\sin[k_Z(Z-ct)+\theta_1]\\ &+\frac{\eta_2U^2}{(1+4\eta_1^2)(1+\eta_1^2)^{\frac{1}{2}}}\cos[2k_Z(Z-ct)+2\theta_1+\theta_2], \end{aligned} \tag{11}$$

where $\eta_1=\overline{K}_1/\rho c\omega$, $\eta_2=\overline{K}_2/\rho c\omega$, $\theta_1=\tan^{-1}(\eta_1^{-1}/2)$, and $\theta_2=\tan^{-1}(\eta_1^{-1})$. The magnitudes of reflection and transmission coefficients are $\Re=(1+4\eta_1^2)^{-1/2}$ and $\Im=2\eta_1(1+4\eta_1^2)^{-1/2}$ (Baik and Thompson, 1984). It is noted that the nonlinear reflection/transmission terms (the amplitudes of the zero-frequency component and the second harmonic) increase with the square of the incident wave amplitude, as is typical result from a system with a weak quadratic nonlinearity.

3. Nonlinearity parameters of an interface

In the finite amplitude nonlinear acoustics, the acoustic nonlinearity parameter for a material is defined as the negative of the ratio of the coefficients of the nonlinear term to the linear term in the nonlinear wave

equation and is thus as the ratio of the third order elastic constant to the second order elastic constant (Breazeale and Philip, 1984). The nondimensional acoustic nonlinearity parameter is a measure of the extent to which the acoustic waveform gets distorted, and so is a direct measure of the nonlinearity of the bulk of a material. It is expressed to be proportional to the ratio of the amplitude of the second order harmonic to the square of the amplitude of the fundamental. As in Cantrell (2004), the acoustic nonlinearity parameter can be defined more generally as the ratio between the coefficients of linear and nonlinear terms in the constitutive equation, which is the actual source of the acoustic nonlinearity of materials.

In the case of interfaces, the nonlinearity parameter may be defined in several different ways depending on what nonlinearity is to be quantified by the parameter. Following Cantrell (2004), the nonlinearity of the interface itself should, of course, be defined to be

$$\beta_I = \frac{\overline{K}_2}{\overline{K}_1} = \frac{\eta_2}{\eta_1}. \tag{12}$$

This parameter is independent of frequency since it is purely a property of the interface; therefore, it is not a measure of the distortion of the reflected or transmitted waves as Eqs. (10) and (11) indicate. One can also define a parameter that quantifies how much nonlinearity was generated out of the incident wave amplitude during the process of wave reflection and transmission. This, as a nonlinear reflection or transmission coefficient, is defined as the ratio of the magnitude of the second harmonic waves to the square of the incident wave amplitude. Since the magnitudes of the second harmonic in the transmitted and reflected waves are equal, this nonlinearity parameter is given commonly to these waves as

$$\beta = \frac{\eta_2}{(1+4\eta_1^2)(1+\eta_1^2)^{\frac{1}{2}}}. \tag{13}$$

On the other hand, the measure of the harmonic distortion in the reflected and transmitted waves can be defined as the ratios of the second harmonic amplitudes to the square of the respective first harmonic amplitudes as in Buck et al. (1978). The nonlinearity parameters for reflected and transmitted waves are

$$\beta_{\mathrm{R}} = \frac{\eta_2}{(1+\eta_1^2)^{\frac{1}{2}}} \tag{14-1}$$

$$\beta_{\mathrm{T}} = \frac{\eta_2}{4\eta_1^2(1+\eta_1^2)^{\frac{1}{2}}}. \tag{14-2}$$

It should be noted that in all above definitions, the nonlinearity parameters related to the interface have the dimensional of $[\mathrm{m}^{-1}]$ while the acoustic nonlinearity parameter for a bulk material is dimensionless. Since the nonlinearity of interface is a property of surface, it has the dimension of one length-scale less than that of the bulk of material. All of these parameters exhibit the hysteretic behavior during the loading cycle but in different manners. For example, β_{I} will show the hysteresis in the motion of the interface while β will display the hysteresis in the second harmonic amplitudes. β and β_{R} (or β_{T}) present respectively an absolute and an relative (to the first harmonic) measure of nonlinearity in the reflected (or transmitted) wave. In this paper, we use these parameters accordingly as relevant.

4. Acoustic (ultrasonic) interfacial stiffness

When acoustic waves interact with an interface, it induces a small-scale loading–unloading cycle centered at a bias static load as shown in Fig. 2. In the elastic contact regime, the acoustic loading–unloading occurs along the static pressure–approach (displacement) curve so that the interfacial stiffness associated with the acoustic wave motion is the same with the static one defined as the slope of the pressure–approach curve at the bias static load. However, when the contacting asperities are plastically deformed, since the unloading occurs following a curve different from the loading curve due to the elastoplastic hysteresis, the acoustically induced loading–unloading cycles should occur along the local unloading curve (Fig. 2). Therefore, the acoustic (ultrasonic) interfacial stiffness between two contacting bodies can be defined more generally as the local unloading

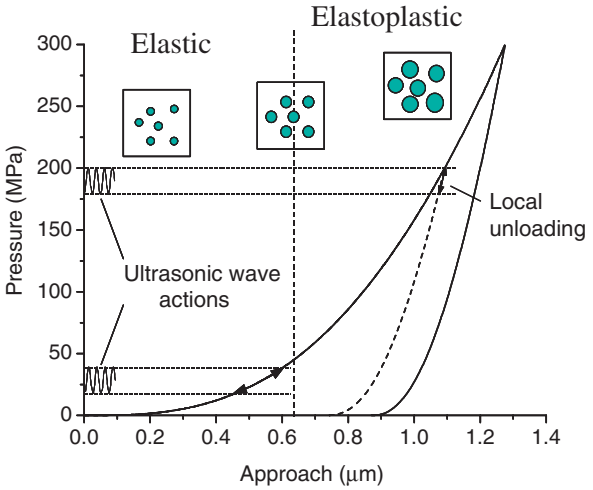

Fig. 2. Pressure–approach curve for two rough surfaces in elastic–elastoplastic contact. The relations of the static and acoustic (ultrasonic) interfacial stiffness to the slope of the pressure–approach curve are illustrated.

stiffness regardless of whether the deformation is elastic or elastoplastic. The acoustic interfacial stiffness is always greater than the static loading interfacial stiffness in the elastoplastic regime. It is because, in the elastoplastic regime, the asperities have a reduced static stiffness due to the progressive plastic deformation while the acoustic stiffness corresponds to the local unloading "elastic" slope and thus its increase is solely due to the increased contact area (Fig. 2). When the unloading starts, the acoustic interfacial stiffness decreases continuously from its maximum at the maximum load as observed by ultrasonic measurements (Drinkwater et al., 1996; Dwyer-Joyce et al., 2001; Baltazar, 2002) whereas the static stiffness has a discontinuity (a jump to the unloading stiffness) at the maximum load.

Now the first and second order interfacial stiffness in Eq. (8) are redefined in a more accurate way,

$$\overline{K}_1 = -\frac{\partial \tilde{p}_{\text{unload}}}{\partial \delta}, \tag{15-1}$$

$$\overline{K}_2 = \frac{1}{2}\frac{\partial^2 \tilde{p}_{\text{unload}}}{\partial \delta^2}. \tag{15-2}$$

5. Micromechanical model for elastoplastic contact

A statistical micromechanical model has recently been proposed (Kim et al., 2004) to analyze the hysteretic behavior of the elastoplastic contact of two rough surfaces and the acoustic interfacial stiffness during loading–unloading cycle. The model incorporates an accurate description of the elastoplastic contact (Kogut and Etsion, 2002) of a single pair of representative asperities into the framework of the statistical asperity model of Greenwood and Williamson (1966). The model uses a χ^2-distribution function for the distribution of asperity heights (Baltazar et al., 2002; Kim et al., 2004):

$$\varphi(2m; z) = (sz)^m \mathrm{e}^{-sz}/z\Gamma(m), \tag{16}$$

where $s = \sqrt{m}/\sigma$, σ is the rms roughness of the composite surface profile, defined as $\sigma = [\sigma_1^2 + \sigma_2^2]^{1/2}$, $\sigma_{1,2}$ are rms roughnesses of the individual surface 1 and 2, and z is the coordinate axis attached at the top of the highest asperity directing downwards. This should be distinguished from the macroscopic global coordinate Z in the previous section. The use of the χ^2-distribution function is advantageous in that it can describe any distribution with skewness toward the top of the surface between the exponential (for $m \leqslant 2$) and the Gaussian (at $m \to \infty$).

Using this distribution function for asperity heights, the nominal pressure (the total load on contacting asperities divided by the nominal contact area), and the first and second order interfacial stiffness in Eqs. (15-1) and (15-2) are expressed as functions of approach δ:

$$\bar{p}(\delta) = \bar{n}\int_0^{\delta} P(\delta - z)\varphi(m;z)\mathrm{d}z, \tag{17}$$

$$\bar{K}_1(\delta) = \bar{n}\int_0^{\delta} \kappa_1(\delta - z)\varphi(m;z)\mathrm{d}z, \tag{18}$$

$$\bar{K}_2(\delta) = \bar{n}\int_0^{\delta} \kappa_2(\delta - z)\varphi(m;z)\mathrm{d}z, \tag{19}$$

where $\bar{n}$ is the number of asperities per unit area; the overbar denotes the statistical average of a random physical quantity; $(\delta - z)$ is the deformation of an asperity summit at z by approach δ; $P(\delta)$, $\kappa_1(\delta)$ and $\kappa_2(\delta)$ are the load and the first and second acoustic stiffness of an individual spherical asperity (see Appendix A).

Substituting Eqs. (A.2), (A.8) and (A.9) into Eqs. (17)–(19) and normalizing appropriately, the total pressure and the first and second order acoustic stiffness of the interface during loading are

$$\frac{\bar{p}(\delta')}{E^*} = \frac{4}{3}C_1 r_{\mathrm{p}}^3 R'^2 \bar{n}\sigma^2 \int_0^{\delta'} \left(\frac{\delta' - z'}{\delta'_{\mathrm{c}}}\right)^{\lambda_1} \varphi^*(m;z')\mathrm{d}z', \tag{20}$$

$$\frac{\overline{K}_1(\delta')}{E^*/\sigma} = 2C_2 r_{\mathrm{p}} R' \bar{n}\sigma^2 \int_0^{\delta'} \left(\frac{\delta' - z'}{\delta'_{\mathrm{c}}}\right)^{\lambda_2} \varphi^*(m;z')\mathrm{d}z', \tag{21}$$

$$\frac{\overline{K}_2(\delta')}{E^*/\sigma^2} = C_2\lambda_2 r_{\mathrm{p}}^{-1} \bar{n}\sigma^2 \int_0^{\delta'} \left(\frac{\delta' - z'}{\delta'_{\mathrm{c}}}\right)^{\lambda_2 - 1} \varphi^*(m;z')\mathrm{d}z', \tag{22}$$

where $C_{1,2}$ and $\lambda_{1,2}$ are the elastoplastic contact coefficients defined in Appendix A; r_{p} is the material property related to elastic–plastic transition (also in Appendix A); the prime denotes normalization of length scale variables by the rms roughness of the composite surface (σ), e.g. $R' = R/\sigma$ and $z' = z/\sigma$; $\varphi^*(m;z) = \varphi(m;z)\sigma$. We have used three independent parameters (σ/R, γ, m) where $\gamma = R'\bar{n}\sigma^2$ for reconstructing properties of composite surfaces from the predicted and measured loading–unloading ultrasonic stiffness (Kim et al., 2004). For a given rms roughness, these are the minimal necessary parameters to compute the contact pressure, the acoustic interfacial stiffness and the real area of contact.

To calculate the interfacial stiffness during unloading, first, the deformation state of the asperities at different depths is considered. Since the maximum displacement and load applied vary with depth, the asperities at different depths possess different amounts of plastic deformation. The plastic deformation in the loading phase leads to the flattening of asperity summits, which results in an increased radius of curvature and the residual deformation. These permanent changes in geometry of asperities are fully taken into account in the unloading model. As in Li et al. (2002), it is assumed that the radius of curvature of the asperity remains unchanged during unloading. The radius of curvature $R_{\max}$ at the maximum load is calculated as a function of z, using Eq. (A.3) and applying the parabolic law, $R_{\max}(z) = a_{\max}^2(z)/\delta_{\max}(z)$. Therefore, at the end of the loading phase, all parameters of plastically deformed asperities are known as a function of their initial heights z in the distribution (16). Using Eq. (A.10), the pressure–approach relation during unloading is thus obtained to be

$$\frac{\bar{p}_u(\delta')}{E^*} = \bar{n}\sigma^2 \int_0^{\delta'} \left\langle \left\langle \frac{P_{\max}(z')}{E^*\sigma^2} - \frac{4}{3}\left(R'_{\max}(z')\right)^{\frac{1}{2}}\left[(\delta'_{\max} - z')^{\frac{3}{2}} - (\delta' - z')^{\frac{3}{2}}\right] \right\rangle \right\rangle \varphi^*(m;z')\mathrm{d}z' \tag{23}$$

where the operator $\langle\langle\ \rangle\rangle$ is defined as

$$\langle\langle f \rangle\rangle = \begin{cases} 0 & \text{for } f \leqslant 0, \\ f & \text{for } f > 0. \end{cases} \tag{24}$$

In evaluating integral (23) at a given δ', the contact load $P(z')$ on the asperities at height z' is first calculated (the term in the operator $\langle\langle\ \rangle\rangle$ in Eq. (23)). If it reduces to or below zero, that is, unloaded completely, the asperities at that height are excluded from the calculation of contact pressure. In this way, only load-bearing

asperities are included in the integration accounting for their residual plastic deformations. The radius curvature that is a function of the initial summit height z is included in the integrand. Assuming that the unloading is perfectly elastic, the first and second order interfacial stiffness are calculated by differentiating successively the unloading pressure–approach relation Eq. (23).

6. Elastoplastic hysteresis, linear and nonlinear acoustic responses of interfaces

Numerical calculations have been performed for three interfaces formed by Al 6061-T6 blocks with two different levels of roughness. The properties of these interfaces have been reconstructed (Kim et al., 2004) from the experimental and theoretical interfacial stiffness during the first loading–unloading cycle. The mechanical properties are given in Table 1. The microstructural parameters of the interfaces used in the simulations are presented in Table 2. Here, we introduce newly a plasticity index as a measure of deformability of the interface for the χ^2-distribution of asperity peaks: $\psi = \sqrt{\sigma(1-m^{-1})/\delta_c}$. It is defined such that rougher and softer surfaces have higher plasticity indices in consideration of the effect of the asperity peak distribution. When $m \to \infty$, it recovers the plasticity index that was originally defined for the Gaussian distribution (Greenwood and Williamson, 1966), and for a surface with $m = 2$ which corresponds to the exponential distribution, the plasticity index is smaller than a Gaussian surface by $\sqrt{2}$. The plastic indices for three composite surfaces are also presented in Table 2.

Figs. 3–5 show the elastoplastically induced hysteresis in the reflection and transmission coefficients at 5 and 10 MHz for the three interfaces as a function of nominal pressure during the loading–unloading cycle. Arrows indicate the loading path. Symbols represent data from the ultrasonic experiments (Baltazar, 2002). They are in good agreement with theoretical ones. It can be seen in these figures that the acoustic waves sensitively respond to the elastic–plastic deformation of the interfaces. For example, in the contact of two smooth surfaces (Fig. 3) the transmission coefficient increases rapidly with the load since the surfaces are smooth (the asperities have a larger radius of curvature), and thus the area of contact (conformity of surfaces) increases rapidly. In all three cases, the transmission coefficient during unloading is higher than that in loading due to the increased real area of contact during unloading (see Fig. 9 in our previous paper (Kim et al., 2004)). The imperfectness of the interface is naturally more impedimental to the waves at higher frequencies, the result of which appears as higher reflection and lower transmission at 10 MHz than those at 5 MHz.

Table 1
Mechanical properties of Al 6061-T6 and Al 1100 alloys

Property	Al 6061-T6	Al 1100
Young's modulus, E	71.0 GPa	69.0 GPa
Hardness, H_B	94	38
Yield stress, σ_Y	235 MPa	138 MPa
Poisson's ratio, ν	0.33	0.33
Longitudinal wave speed, c_l	6370 m/s	6350 m/s
Density, ρ	2740 kg/m^3	2740 kg/m^3

Table 2
Model parameters (Kim et al., 2004)

Surface	Given σ[a] (μm)	Reconstructed			Calculated using reconstructed parameters	
		σ/R	γ	m	ψ	p_Y[b] (MPa)
Smooth–smooth	0.325	2.01×10^{-4}	2.4	3.0	1.33	84.6
Rough–smooth	2.4	1.20×10^{-3}	2.62	1.5	2.32	18.4
Rough–rough	3.4	1.92×10^{-3}	1.27	2.0	3.62	3.30

[a] RMS roughness of composite surface.
[b] Nominal pressure at the onset of the plastic deformation at the interface.

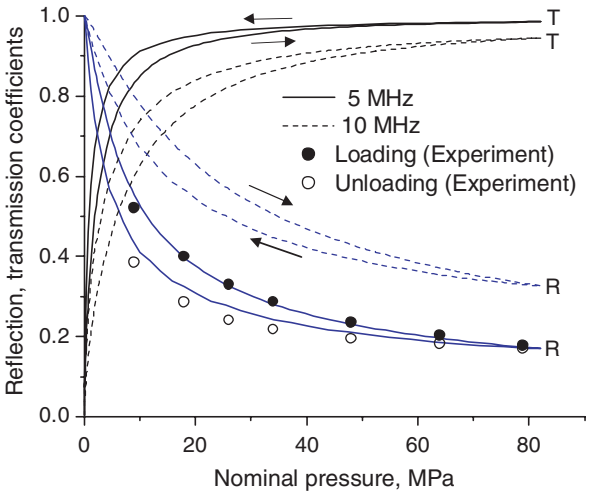

Fig. 3. Hysteresis in reflection and transmission coefficients from the interface formed by two smooth surfaces with rms roughness 0.25 μm. Symbols are experimental results (Baltazar, 2002). The nominal pressure at the onset of the plastic deformation at the interface was predicted to be 84.6 MPa (Kim et al., 2004).

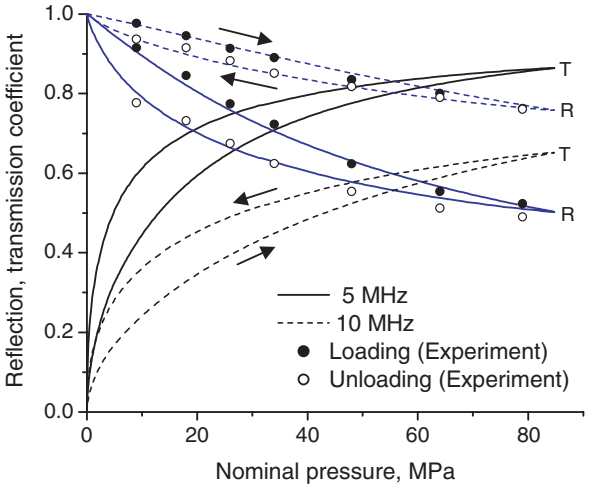

Fig. 4. Hysteresis in reflection and transmission coefficients from the interface formed by a rough (rms roughness 2.4 μm) and a smooth (rms roughness 0.25 μm) surface. Symbols are experimental results (Baltazar, 2002). The nominal pressure at the onset of the plastic deformation at the interface was predicted to be 3.3 MPa (Kim et al., 2004).

The acoustic interfacial stiffness of these interfaces are shown in Fig. 6. Among three interfaces, the interface between two smooth surfaces has the smallest plasticity index, allowing the plastic yielding to occur only at the end of loading, mostly in the asperities near the surface. This interface, however, exhibits the highest level of hysteresis in the interfacial stiffness. In the interface formed by rough–rough surfaces, the plastic deformation starts at a low load ($p_Y = 3.3$ MPa) due to its high plasticity index ($\psi = 3.62$) and the external load is supported by the flattened asperities that are highly populated near the top surface ($m = 2$: the exponential distribution). This interface shows the lowest level of hysteresis. It is interesting to note that the hysteresis levels in the interfacial stiffnesses are in reverse order of those in the load–displacement curves for the same three interfaces (see Fig. 10 in Kim et al. (2004)). A similar effect is observed in the hysteresis of the nonlinearity presented in the followings.

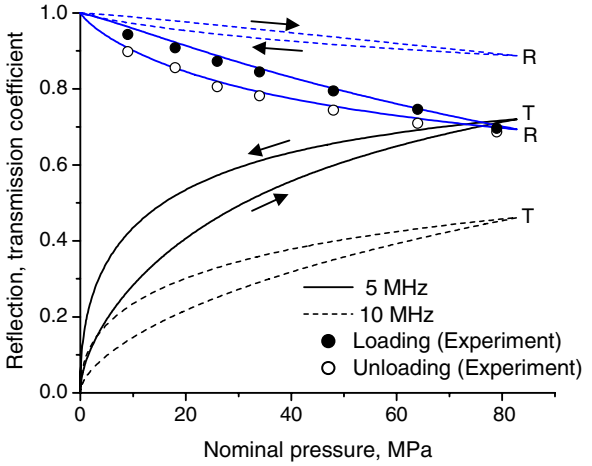

Fig. 5. Hysteresis in reflection and transmission coefficients from the interface formed by two rough surfaces with rms roughness 2.4 μm. Symbols are experimental results (Baltazar, 2002). The nominal pressure at the onset of the plastic deformation at the interface was predicted to be 18.4 MPa (Kim et al., 2004).

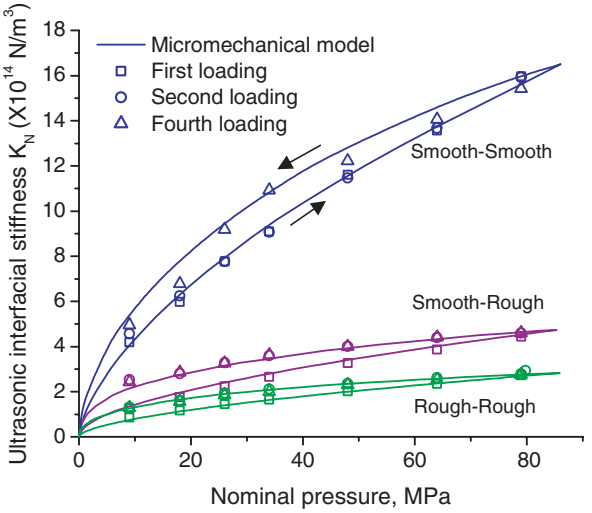

Fig. 6. Hysteresis in ultrasonic interfacial stiffnesses of the three different interfaces. Symbols are experimental results (Baltazar, 2002).

Figs. 7–9 show the nonlinearity parameters defined by Eqs. (12) and (13) for the three different interfaces. Several interesting things can be noted. First, in both β_I and β the elastoplastic hysteresis is most pronounced in the contact of two smooth surfaces. Similarly, the hysteresis of the interface between smooth and rough surfaces is higher than that of rough–rough surfaces. This paradoxical fact observed commonly in the hysteresis of the interfacial stiffness and the nonlinear parameters can be explained as followings: The interfacial stiffness and the acoustic nonlinearity of an elastic interface are much higher than those of a plastically deformed interface as shown in Figs. 6–9. In the contact of two smooth surfaces where the plastic yielding takes place at the end of loading, the asperities are elastically deformed during loading while they remains plastically deformed during unloading. Therefore, the interfacial stiffness and the nonlinearity change significantly from those of elastic ones to those of plastic ones. On the contrary, in the contact of two rough surfaces, since the plastic yielding starts at a low load level, the interfacial stiffness and the nonlinearity during loading and unloading are similar, that is, plastically deformed, which causes little change in the interfacial stiffness and the nonlinearity, and thus the smallest hysteresis. In all cases, the acoustic nonlinearity during unloading

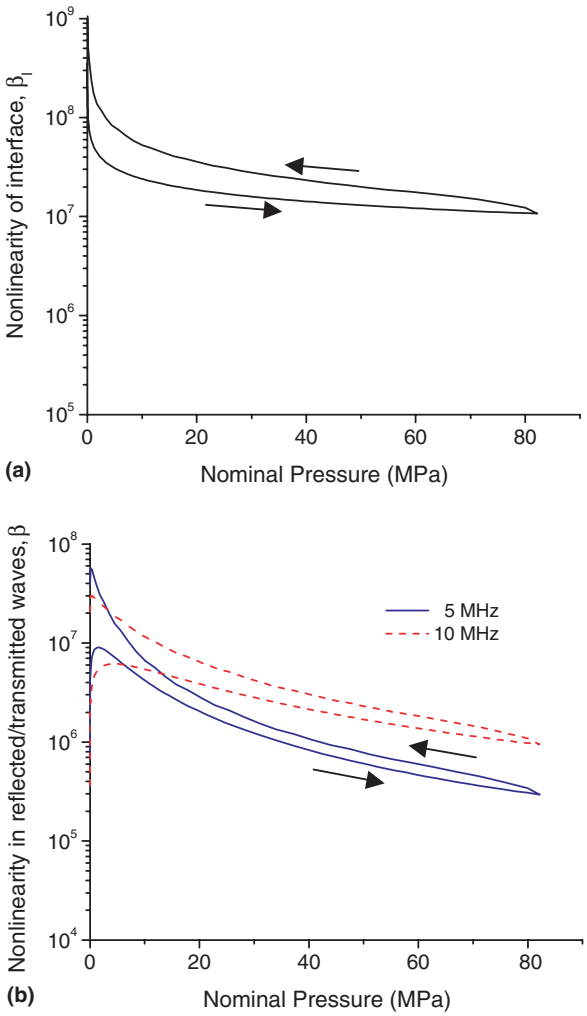

Fig. 7. Hysteretic behavior in the acoustic nonlinearity: (a) the nonlinearity of interface (β_I); (b) the nonlinearity in reflected/transmitted waves (β) for the interface formed by two smooth surfaces. The parameters of surface topography are the same as in Fig. 3.

exhibits a history-dependent behavior whenever inelastic deformation occurs. Most eminently, if the maximum pressure on the smooth–smooth interface was below 84.6 MPa the pressure at onset of plastic yielding, the interface would not have shown any hysteresis.

From β for three different interfaces, it is observed that the nonlinearity of the interface decreases by more than an order of magnitude (>20[1] dB) during the transition from the elastic contact mode into the elastoplastic contact mode in the present material (Al-6061). Once the plastic deformation occurs, the nonlinearity remains nearly constant. For a given interface, the nonlinearity seems to be always higher during unloading than during loading. From these, it may be concluded that a lightly loaded smooth interface generates most efficiently the nonlinearity in the scattered waves. The nonlinearity of interface β_I also exhibits a rapid initial drop at lower contact pressures. Since the static pressure can be written approximately as $p_0 \sim \delta_0^{\lambda_1+1}$ (from Eq. (20)), the total pressure is $p_0 + \tilde{p} \sim (\delta_0 + \tilde{\delta})^{\lambda_1+1}$. The pressure disturbance in the interface by the action of acoustic waves is expanded near the static pressure,

[1] This figure may have the dependence on the hardness of materials.

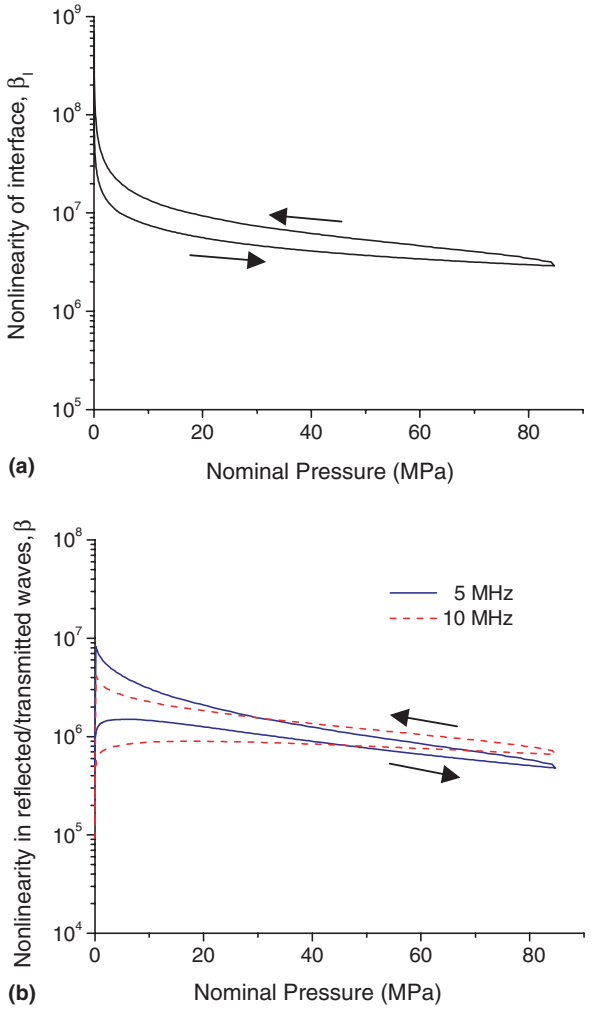

Fig. 8. Hysteretic behavior in the acoustic nonlinearity: (a) the nonlinearity of interface (β_I); (b) the nonlinearity in reflected/transmitted waves (β) for the interface formed by a rough and a smooth surface. The parameters of surface topography are the same as in Fig. 4.

$$\tilde{p} \sim (\lambda_1 + 1)\delta_0^{\lambda_1}\tilde{\delta}\left(1 + \frac{\lambda_1}{2}\frac{\tilde{\delta}}{\delta_0} + \cdots\right) \approx -\overline{K}_1\tilde{\delta}(1 - \beta_I\tilde{\delta}). \tag{25}$$

This equation indicates that the nonlinearity of the interface is inversely proportional to the static displacement or the nominal contact pressure, which explains the initial drop of β_I. In practice, however, instead of the indefinite increase of nonlinearity with decreasing pressure, a complete separation and clapping motion of two surfaces can be induced, which is another mode of nonlinear hysteretic motion (Solodov et al., 1993; Moussatov et al., 2003). The nonlinearity due to the clapping motion has been observed to be a maximum at a low pressure also. Considering the low transmission coefficient at low contact pressures, the transmitted wave amplitude in this regime is mostly due to the second harmonic wave.

Fig. 10 shows the dependence of the acoustic nonlinearity (β_T) in the transmitted wave on the surface topographic parameters; surface roughness, peak distribution (m) and the plasticity index. An Al 1100 alloy used in the simulation, the properties of which are presented in Table 1. To reduce the number of variables, other surface parameters are fixed: $\gamma = 2.5$ and $R' = 1000$. Three dashed lines show the effect of peak distribution on the nonlinearity for the surfaces having the same roughness $\sigma = 3.5$ μm. From Table 2, $\sigma = 3.5$ μm represents a quite rough interface, therefore, the plastic deformation at asperity peaks should be prevalent. In these

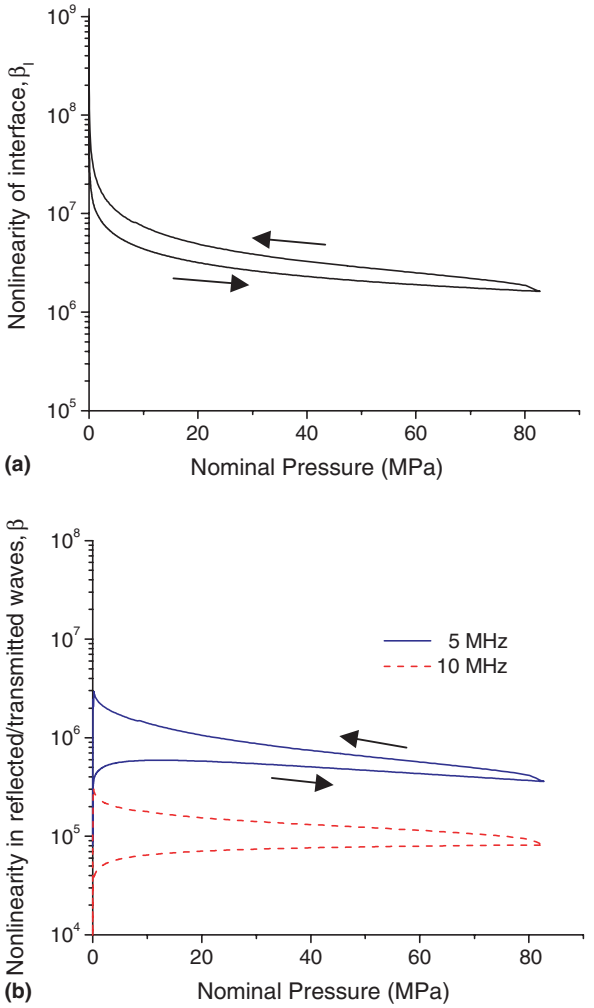

Fig. 9. Hysteretic behavior in the acoustic nonlinearity: (a) the nonlinearity of interface (β_I); (b) the nonlinearity in reflected/transmitted waves (β) for the interface formed by two rough surfaces. The parameters of surface topography are the same as in Fig. 5.

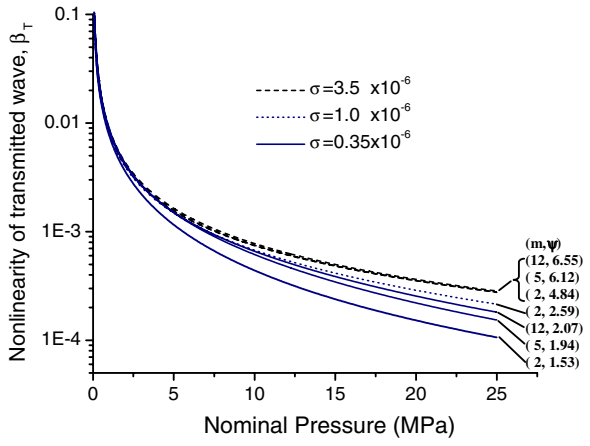

Fig. 10. Dependence of acoustic nonlinearity parameter β_T on the surface roughness, asperity peak distribution and the plasticity index.

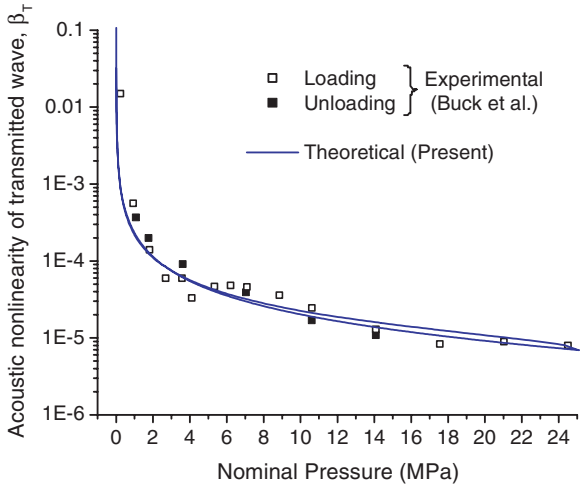

Fig. 11. The acoustic nonlinearity parameter β_T from an interface between two Al 1100 blocks during the loading–unloading cycle. Symbols (open and solid squares): experimental data from Buck et al. (1978); solid line: the present theoretical model.

interfaces, the nonlinearity exhibits no sensitivity to the asperity peak distribution, which results in a near coincidence of the three dashed lines. On the contrary, when $\sigma = 0.35$ μm which corresponds to a quite smooth interface, the effect of asperity peak distribution is notable. From these, it can be concluded that the determination of roughness height distribution through the measurements of acoustic nonlinearity as intended by Rudenko and Vu (1994) is possible only when the contacting surfaces are smooth making the elastic deformation dominant ($\psi < 3$). Nonetheless, it may be further limited to a situation in which the surface roughness can accurately be measured. Otherwise, as shown in Fig. 10, three surfaces with the same distribution ($m = 2$) but with different surface roughness show much larger variation.

In Fig. 11, the experimental results of Buck et al. (1978) for the nonlinearity of elastic waves transmitted through an interface between two Al 1100 blocks are compared with the theoretical prediction. Since no data on the material properties and on the surfaces are available in their paper, a typical set of material properties listed in Table 1 is used in the calculation. The theoretical curve was scaled by a constant multiplier since y-axis (A_2/A_1^2) is in arbitrary unit (most likely the electrical signal amplitudes of the first and second harmonics were not calibrated). The first observation from the measurement results is that there is no change in the nonlinearity during loading and unloading, indicative of a significant plastic deformation started at a low pressure as we found already from Figs. 7–9. The elastoplastic hysteresis is probably small enough to fall well in the range of the measurement error. The parameters used in the calculation are: $\sigma = 2.4$ μm, $\gamma = 9.8$, $m = 10$, $R' = 2000$ and the resulting plasticity index is $\psi = 5.38$. It should be noted that, in spite of the apparently excellent agreement, the theoretical curve shown is just one of many possible best-fits. In other words, as shown in Fig. 10, due to the coincidence of the acoustic nonlinearity curves of transmitted waves for interfaces with high plastic flow, there may be not only one but many curves from different sets of parameters that can fit the experimental data. Due to this fact, Biwa et al. (2004) were able to fit this data set with the parameters of the simple power-law determined from the other experimental data for a different material (Drinkwater et al., 1996) but undergoing significant plastic flow at the interface. Therefore, the reduction of the complicated problem using the simple power-law dependence for the pressure–approach relation is valid when there is a significant plastic deformation at the interface so that the self-similarity of inelastic contact (Storakers et al., 1997) supports the power-law.

7. Summary

The linear and second order acoustic stiffness of an interface under a compressive stress are calculated from the micromechanical elastoplastic contact model to predict the acoustic nonlinearity of the interface during the

first loading–unloading cycle. The hysteretic linear and nonlinear acoustic responses from interfaces with different microstructures are predicted. The second order harmonic amplitude of reflected/transmitted waves as indicated by β decreases by more than an order of magnitude during the transition of the elastic–plastic deformation. An interesting phenomenon of loading-history dependent acoustic nonlinearity during the unloading phase is observed. For the combination of loading-history and interface properties considered here, the interface between smooth surfaces can exhibit higher elastoplastic hysteresis in interfacial stiffness and nonlinearity than the interface between rough surfaces. The different asperity distributions in the interfaces with high plasticity indices do not make distinguishable change in the acoustic nonlinearity. The present model can be useful for modeling nonlinear and hysteretic behaviors of imperfect interfaces and cracks and their ultrasonic nondestructive evaluation based on probing these phenomena.

Acknowledgements

J.W. Hu would like to thank KOSEF for financial support. The authors thank Ms. Aracely Baltazar for proofreading the manuscript.

Appendix A. Loading–unloading of single asperity contact

Consider two identical deformable spheres with radius R, Young's modulus E, Poisson's ratio v and yield stress σ_Y. The spheres are pressed by an external load P to be in normal contact producing a relative normal approach δ. The critical approach δ_c at which a local plastic yielding commences (yielding inception) (Chang et al., 1987) is given by

$$\delta_c = r_p^2 R, \tag{A.1}$$

where $r_p = (\pi k H/2E^*)$; $E^* = E/(1-v^2)$; H is the hardness of the material (Tabor, 1951); k the hardness coefficient is given by $k = 0.454 + 0.41v$ (Kogut and Etsion, 2002). The normalized load and the radius of contact area versus the normalized approach can be represented in a unified way:

$$\frac{P}{P_c} = C_1 \left(\frac{\delta}{\delta_c}\right)^{\lambda_1}, \tag{A.2}$$

$$\frac{a}{a_c} = C_2 \left(\frac{\delta}{\delta_c}\right)^{\lambda_2}, \tag{A.3}$$

where a is the contact radius, P_c and a_c are the load and the radius of contact area at the yield inception given by Hertz theory (Johnson, 1985),

$$P_c = \frac{4}{3} E^* R^{\frac{1}{2}} \delta_c^{\frac{3}{2}}, \tag{A.4}$$

$$a_c = (R\delta_c)^{\frac{1}{2}}, \tag{A.5}$$

and $C_{1,2}$ and $\lambda_{1,2}$ are coefficients for different contact regimes. Recently, an accurate finite element analysis of the elastoplastic contact of two spheres (Kogut and Etsion, 2002) provides the coefficients in Eqs. (A.2) and (A.3): $C_1 = C_2 = 1$, $\lambda_1 = 1.5$ and $\lambda_2 = 0.5$ for $\delta/\delta_c \leqslant 1$; $C_1 = 1.03$, $C_2 = 0.96$, $\lambda_1 = 1.425$, $\lambda_2 = 0.568$ for $1 \leqslant \delta/\delta_c \leqslant 6$; $C_1 = 1.40$, $C_2 = 0.97$, $\lambda_1 = 1.263$, $\lambda_2 = 0.573$ for $6 \leqslant \delta/\delta_c \leqslant 110$. Since the coefficients are those for dimensionless expressions (Eqs. (A.2) and (A.3)), they are not restricted to a specific material or sphere radius.

To calculate the acoustic interfacial stiffness of a single asperity, the local unloading slope is first obtained. At any point of the loading curve the slope of the initial unloading curve ($\partial P_{unload}/\partial\delta$) and the acoustic stiffness of the single asperity may be calculated (Johnson, 1996; Cheng and Cheng, 1997; Oliver and Pharr, 1992) as

$$\frac{\partial P_{unload}}{\partial \delta} = 2aE^*, \tag{A.6}$$

where the elastoplastic radius of the contact area a is obtained from the loading model Eq. (A.3). Thus, the acoustic interfacial stiffness during loading for the single asperity is

$$\kappa_1 = \frac{\partial P_{\text{unload}}}{\partial \delta} = 2aE^*. \tag{A.7}$$

Substituting Eq. (A.3) into Eq. (A.7) and differentiating, one obtains

$$\kappa_1 = 2C_2E^*a_c\left(\frac{\delta}{\delta_c}\right)^{\lambda_2}, \tag{A.8}$$

$$\kappa_2 = C_2\lambda_2E^*a_c\delta_c^{-1}\left(\frac{\delta}{\delta_c}\right)^{\lambda_2-1}. \tag{A.9}$$

Since the unloading process is predominantly elastic the slope at any point on the full unloading curve from the maximum load to zero is given by Eq. (A.6) (Johnson, 1996). However, the relationship between the displacement (δ) and the radius of contact area (a) is generally unknown during the recovery from an arbitrary plastic state. Therefore, to use it along the whole unloading curve an approximate unloading model is required for calculating the stiffness from the above equation. An approximate unloading model can be evaluated by checking if it satisfies the fundamental relationship Eq. (A.6). As in Kim et al. (2004), the unloading model of Li et al. (2002) is employed. The load–displacement relation during unloading is given

$$\frac{P}{P_c} = \frac{P_{\max}}{P_c} - \left(\frac{R_{\max}}{R}\right)^{\frac{1}{2}}\left[\left(\frac{\delta_{\max}}{\delta_c}\right)^{\frac{3}{2}} - \left(\frac{\delta}{\delta_c}\right)^{\frac{3}{2}}\right], \tag{A.10}$$

where $P_{\max}$ and $\delta_{\max}$ are the maximum load and the corresponding maximum approach during loading–unloading cycle; $R_{\max}$ is the radius of curvature at the maximum load.

References

Baik, J.M., Thompson, R.B., 1984. Ultrasonic scattering from imperfect interfaces. J. Nondestr. Eval. 4, 177–196.

Baltazar, A., 2002. Ultrasonic wave interaction with imperfect interfaces. PhD Dissertation, The Ohio State University.

Baltazar, A., Rokhlin, S.I., Pecorari, C., 2002. On the relation between ultrasonic micromechanic properties of contacting rough surfaces. J. Mech. Phys. Solids 50, 1397–1416.

Biwa, S., Nakajima, S., Ohno, N., 2004. On the acoustic nonlinearity of solid–solid contact with pressure-dependent interface stiffness. J. Appl. Mech. 71, 508–515.

Breazeale, M.A., Philip, J., 1984. Determination of their-order elastic constants from ultrasonic harmonic generation measurements. Phys. Acoust. 17, 1–60.

Buck, O., Morris, W.L., Richardson, J.M., 1978. Acoustic harmonic generation at unbonded interfaces and fatigue cracks. Appl. Phys. Lett. 33, 371–373.

Cantrell, J.H., 2004. Substructural organization, dislocation plasticity and harmonic generation in cyclically stressed wavy slip metals. Proc. Roy. Soc. Lond., Ser. A 460, 757–780.

Chang, W.R., Etsion, I., Bogy, D.B., 1987. An elastic–plastic model for the contact of rough surfaces. ASME J. Tribol. 109, 257–263.

Chen, J., Jiang, W., Shui, Y., 2001. Observation of nonlinear acoustic effects at isotropic solid–solid interfaces. J. Acoust. Soc. Am. 109, 501–507.

Cheng, C.-M., Cheng, Y.-T., 1997. On the initial unloading slope in indentation of elastic–plastic solids by an indentor with an axisymmetric smooth profile. Appl. Phys. Lett. 71, 2623–2625.

Donskoy, D., Sutin, A., Ekimov, A., 2001. Nonlinear acoustic interaction on contact interfaces and its use for nondestructive testing. NDT&E Int. 34, 231–238.

Drinkwater, B., Dwyer-Joyce, R., Cawley, P., 1996. A study of the interaction between ultrasound and a partially contacting solid–rubber solid interface. Proc. Roy. Soc. Lond., Ser. A 452, 2613–2628.

Dwyer-Joyce, R.S., Drinkwater, B.W., Quinn, A.M., 2001. The use of ultrasound in the investigation of rough surface interfaces. ASME Trans. J. Tribol. 123, 8–16.

Fassbender, S.U., Arnold, W., 1996. Measurement of adhesion strength of bonds using nonlinear acoustics. In: Thompson, D.O., Chimenti, D.E. (Eds.), Rev. Prog. Quant. Nondestruc. Eval., vol. 15. Plenum Press, New York, pp. 1321–1328.

Greenwood, J.A., Williamson, J., 1966. Contact of nominally flat surfaces. Proc. R. Soc. Lond., Ser. A 295, 300–319.

Gusev, V., Castagnede, B., Moussatov, A., 2003. Hysteresis in response of nonlinear bistable interface to continuously varying acoustic loading. Ultrasonics 41, 643–654.

Hirsekorn, S., 2001. Nonlinear transfer of ultrasound by adhesive joints—a theoretical description. Ultrasonics 39, 57–68.

Hirose, S., Achenbach, J.D., 1993. Higher harmonics in the far field due to dynamic crack-face contacting. J. Acoust. Soc. Am. 93, 142–147.

Johnson, K.L., 1985. Contact Mechanics. Cambridge University Press, Cambridge.

Johnson, K.L., 1996. Modelling the indentation hardness of solids. In: Proceedings of the First Royal Society-Unilevel Indo-Uk Forum in Material Science and Engineering, Solid–Solid Interactions. Imperial College Press, pp. 16–28.

Kim, J.-Y., Baltazar, A., Rokhlin, S.I., 2004. Ultrasonic assessment of rough surface contact between solids from elastoplastic loading–unloading hysteresis cycle. J. Mech. Phys. Solids 52, 1911–1934.

Kogut, L., Etsion, I., 2002. Elastic–plastic contact analysis of a sphere and a rigid flat. J. Appl. Mech. 69, 657–662.

Li, L.-Y., Wu, C.-Y., Thornton, C., 2002. A theoretical model for the contact of elastoplastic bodies. Proc. Instn. Mech. Engrs. 216 (Part C), 421–431.

Moussatov, A., Gusev, V., Castagnede, B., 2003. Self-induced hysteresis for nonlinear acoustic waves in cracked materials. Phys. Rev. Lett. 90, 124301-1–124301-4.

Nagy, P.B., 1992. Ultrasonic classification of imperfect interfaces. J. Nondestruct. Eval. 11, 127–140.

Nazarov, V.E., Sutin, A., 1997. Nonlinear elastic contacts of solids with cracks. J. Acoust. Soc. Am. 102, 3349–3354.

Needleman, A., 1990. An analysis of tensile decohesion along an interface. J. Mech. Phys. Solids 38, 289–324.

Oliver, W.C., Pharr, G.M., 1992. An improved technique for determining hardness and elastic modulus using load and displacement sensing indentation experiments. J. Mater. Res. 7, 1564–1583.

Pecorari, C., 2003. Nonlinear interaction of plane ultrasonic waves with an interface between rough surfaces in contact. J. Acoust. Soc. Am. 113, 3065–3072.

Richardson, J.M., 1979. Harmonic generation at an unbonded interface—I. Planar interface between semi-infinite elastic media. Int. J. Eng. Sci. 17, 73–85.

Rokhlin, S.I., Wang, Y.J., 1991. Analysis of boundary conditions for elastic wave interaction with an interface between two solids. J. Acoust. Soc. Am. 89, 503–515.

Rokhlin, S.I. (Ed.), 1992. Special issue on modeling and ultrasonic characterization of interfaces. J. Nondestruc. Eval., vol. 11.

Rokhlin, S.I., Kim, J.-Y., 2003. In situ ultrasonic monitoring of surface fatigue crack initiation and growth from surface cavity. Int. J. Fatigue 25, 41–49.

Rudenko, O.V., Vu, C.A., 1994. Nonlinear acoustic properties of a rough surface contact and acoustodiagnostics of a roughness height distribution. Acoust. Phys. 40, 593–596.

Solodov, I.Y., Asainov, A.F., Len, K.S., 1993. Non-linear SAW reflection: experimental evidence and NDE application. Ultrasonics 36, 91–96.

Solodov, I.Y., Korshak, B.A., 2002. Instability, chaos, and "memory" in acoustic-wave-crack interaction. Phys. Rev. Lett. 88, 014303–014305.

Storakers, B., Biwa, S., Larsson, P.-L., 1997. Similarity analysis of inelastic contact. Int. J. Solids Struct. 34, 3061–3083.

Suo, Z., Ortiz, M., Needleman, A., 1992. Stability of solids with interfaces. J. Mech. Phys. Solids 40, 613–640.

Tabor, D., 1951. The Hardness of Metals. Oxford University Press.